

Thermal behavior of Bose-Einstein condensates of polar molecules

J. Sánchez-Baena,^{1,*} G. Pascual,¹ R. Bombín,² F. Mazzanti,¹ and J. Boronat¹

¹Departament de Física, Universitat Politècnica de Catalunya, Campus Nord B4-B5, 08034 Barcelona, Spain

²Université de Bordeaux, 351 Cours de la Libération, 33405 Talence, France

(Dated: October 17, 2025)

We use the finite-temperature extended Gross-Pitaevskii equation (TeGPE) to study a condensate of dipolar NaCs molecules under the conditions of the very recent, breakthrough experiment [Bigagli *et al.*, *Nature* **631**, 289 (2024)]. We report the condensate fraction of the system, and its density profile after a time-of flight expansion for the coldest experimental case, finding excellent agreement with the experimental measurements. We also report the peak density of the ground state and establish a comparison with the experimental estimates. Our results, derived from the TeGPE formalism, successfully describe the Bose-Einstein condensation of polar molecules at finite temperature.

I. INTRODUCTION

The recent progress in the control and reduction of reactive losses for ultracold dipolar molecules [1–5] has culminated in the first realization of a Bose-Einstein condensate (BEC) of dipolar molecules [6], which represents a major breakthrough in the field. While the condensate still lies in the dilute regime, it represents the first step towards the realization of highly correlated, dipole-dominated molecular systems [7]. In fact, the physics of ultracold quantum dipolar atomic gases has been the subject of intense experimental and theoretical activity in the last decade. This is due to the unique combination of traits of the dipole-dipole interaction (DDI), mainly its anisotropy and long-range behavior. Due to the high controllability achievable with ultracold quantum gases, dipolar systems represent the perfect testbed to study the wide variety of physical phenomena that arises thanks to their unique properties. This includes, most notably, the emergence of ultradilute liquid dipolar droplets with magnetic atoms [8–12], supersolids [13–21] or anomalous thermal behavior [21–24], to name a few. At present, the vast majority of experiments on dipolar gases have been realized using highly magnetic atoms, like Dysprosium [25] or Erbium [26]. However, in these systems, the regime in which dipolar interactions dominate is restricted to low values of the gas parameter, $\rho a^3 \lesssim 10^{-4}$ (with ρ the density and a the s-wave scattering length), where the system is very dilute. Increasing n leads to the enhancement of three-body losses, while increasing a implies that short-range interactions take over the DDI, thus washing out dipolar effects.

The physics of dipolar quantum gases can be drastically changed if one considers dipolar molecules instead of magnetic atoms. This is because dipolar molecules have a much higher dipolar strength (from 10 to 1000 times bigger than in ^{164}Dy), thus allowing for a drastic increase of a (and consequently, the gas parameter) without losing dipolar physics. The experimental achievement of

a BEC of molecules [6] also represents an excellent opportunity to benchmark the validity of Bogoliubov theory and the finite-temperature extended Gross Pitaevskii equation (TeGPE) for the theoretical description of these novel systems. Remarkably, recent results in the strongly correlated, dipole-dominated limit show the failure of the eGPE to reproduce quantum Monte Carlo results for the critical number required to form molecular droplets [7]. However, it has not been addressed how accurate the TeGPE is in the specific conditions of the experiment of Ref. [6], which lays far away from the highly correlated regime.

Temperature is a key parameter in the theoretical description of the molecular condensate achieved in the experiment, since only a maximum condensate fraction of $\sim 60\%$ was achieved. Therefore, there is an important thermal depletion of the BEC that the state-of-the-art theoretical approach, the zero temperature extended Gross-Pitaevskii equation, is not able to describe [22, 27–31]. In fact, recent experimental and theoretical results have shown that thermal effects play a rather counterintuitive role in dipolar systems by the promotion of supersolidity by heating [21–24]. Nevertheless, the study of dipolar systems at finite temperature is a rather unexplored topic, and as a consequence it is important to test and benchmark the regime of validity of the available theoretical tools, especially in the context of polar molecules.

II. SYSTEM AND METHODS

A. The temperature extended Gross Pitaevskii equation (TeGPE)

In this work, we employ Bogoliubov theory and the local density approximation (LDA) to account for thermal fluctuations on the condensate [22, 30, 31]. We aim to study ensembles of NaCs molecules under the same conditions of the recent experiment of Ref. [6]. We employ the temperature dependent extended Gross-Pitaevskii equation (TeGPE) for the condensate wave function $\psi(\mathbf{r})$

* juan.sanchez.baena@upc.edu

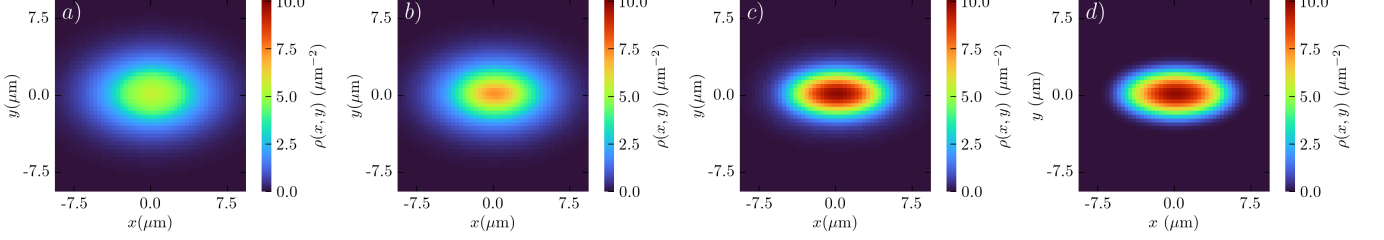


FIG. 1. Emergence of a molecular Bose Einstein Condensate as the temperature is lowered. The panels depict the column density $\rho(x, y) = \int dz (|\psi(\mathbf{r})|^2 + \rho_d(\mathbf{r}))$, with $\psi(\mathbf{r})$ the condensate wave function and $\rho_d(\mathbf{r})$ the density of depleted molecules. The total number of molecules is $N = 298$, while the temperatures are $T = 10.5, 9.5, 6$ and 0 nK for panels *a*) to *d*), respectively. The condensate fractions for each case are $f_c = 0.01, 0.12, 0.58$ and 0.96 , respectively. Panel *c*) corresponds to the coldest point of the experiment of Ref. [6].

given by

$$\begin{aligned} \mu\psi(\mathbf{r}) = & \left(-\frac{\hbar^2 \nabla^2}{2m} + U(\mathbf{r}) + \int d\mathbf{r}' V(\mathbf{r} - \mathbf{r}') \right. \\ & \times \left. [|\psi(\mathbf{r}')|^2 + \rho_d(\mathbf{r}')] + H_{\text{qu}}(\mathbf{r}) + H_{\text{th}}(\mathbf{r}) \right) \psi(\mathbf{r}) . \end{aligned} \quad (1)$$

In this expression, μ is the chemical potential, m is the molecular mass, $V(\mathbf{r}) = V_{\text{dd}}(\mathbf{r}) + \frac{4\pi\hbar^2 a}{m} \delta(\mathbf{r})$ stands for both the contact and dipole-dipole interactions, a is the s-wave scattering length, and $\rho_d(\mathbf{r})$ is the density of molecules out of the BEC state. The term $U(\mathbf{r}) = \frac{1}{2}m(\omega_x^2 x^2 + \omega_y^2 y^2 + \omega_z^2 z^2)$ is the harmonic trap. In the experiment of Ref. [6], the orientation of the molecular dipoles could not be determined. Nevertheless, we consider the dipoles to be polarized along the z -axis, and show that our results are robust with respect to variations of this direction (see Sec. III D). The dipole-dipole interaction is given by

$$V_{\text{dd}}(\mathbf{r}) = \frac{d_{\text{eff}}^2}{4\pi\epsilon_0} \left(\frac{1 - 3\cos^2\theta}{r^3} \right) , \quad (2)$$

where $\mathbf{r} = \mathbf{r}_i - \mathbf{r}_j$, $r = |\mathbf{r}|$, θ is the angle between the vector \mathbf{r} and the z axis, d_{eff} is the effective dipole moment and ϵ_0 is the permittivity of free space. The terms H_{qu} and H_{th} of Eq. 1 account for the effect of quantum and thermal fluctuations, respectively. The first term is given by the usual Lee-Huang-Yang expression [32, 33]

$$H_{\text{qu}}(\mathbf{r}) = \frac{32}{3\sqrt{\pi}} g \sqrt{a^3} Q_5(a_{\text{dd}}/a) |\psi(\mathbf{r})|^3 . \quad (3)$$

The parameter $a_{\text{dd}} = md_{\text{eff}}^2/(12\pi\hbar^2\epsilon_0)$ corresponds to the dipole length and the auxiliary function $Q_5(a_{\text{dd}}/a)$ is given by [33]

$$Q_5(a_{\text{dd}}/a_s) = \int_0^1 du \left(1 - \frac{a_{\text{dd}}}{a_s} + 3 \left(\frac{a_{\text{dd}}}{a_s} \right) u^2 \right)^{5/2} . \quad (4)$$

The correction by thermal fluctuations in Eq. 1 is given by

$$H_{\text{th}}(\mathbf{r}) = \int \frac{d\mathbf{k}}{(2\pi)^3} \frac{V(\mathbf{k})}{(e^{\beta\varepsilon_{\mathbf{k}}} - 1)} \left[|u_{\mathbf{k}}|^2 + |v_{\mathbf{k}}|^2 - 2|u_{\mathbf{k}}||v_{\mathbf{k}}| \right] , \quad (5)$$

where $V(\mathbf{k})$ is the Fourier transform of the DDI plus contact potential, $u_{\mathbf{k}}$ and $v_{\mathbf{k}}$ are the Bogoliubov amplitudes while $\beta = 1/k_B T$.

B. Calculation of the Bogoliubov amplitudes

We take the following considerations in the calculation of the thermal correction to the eGPE, i.e. the $H_{\text{th}}(\mathbf{r})$ term of Eq. 5. The fact that the experimental condensate that we aim to describe lies in the regime $a > a_{\text{dd}}$, meaning that the system is stable at the mean field level, allows us to account for the curvature of the condensate for vanishing densities, i.e. near the edges of the trap. This allows us to modify the usual calculation under the LDA for dipolar systems [22, 30, 31] to obtain a convergent thermal depletion. Under these circumstances, the Bogoliubov de-Gennes equations for the excitations are

$$\begin{aligned} E_{\mathbf{k}} u_{\mathbf{k}}(\mathbf{r}) = & \left(\frac{\hbar^2 k^2}{2m} + U(\mathbf{r}) - \mu_{\text{MF}} \right) u_{\mathbf{k}}(\mathbf{r}) \\ & + u_{\mathbf{k}}(\mathbf{r}) \int d\mathbf{r}' V(\mathbf{r} - \mathbf{r}') |\psi_{\text{MF}}(\mathbf{r}')|^2 \\ & + |\psi_{\text{MF}}(\mathbf{r})|^2 u_{\mathbf{k}}(\mathbf{r}) V(\mathbf{k}) - |\psi_{\text{MF}}(\mathbf{r})|^2 v_{\mathbf{k}}(\mathbf{r}) V(\mathbf{k}) \end{aligned} \quad (6)$$

$$\begin{aligned} -E_{\mathbf{k}} v_{\mathbf{k}}(\mathbf{r}) = & \left(\frac{\hbar^2 k^2}{2m} + U(\mathbf{r}) - \mu_{\text{MF}} \right) v_{\mathbf{k}}(\mathbf{r}) \\ & + v_{\mathbf{k}}(\mathbf{r}) \int d\mathbf{r}' V(\mathbf{r} - \mathbf{r}') |\psi_{\text{MF}}(\mathbf{r}')|^2 \\ & + |\psi_{\text{MF}}(\mathbf{r})|^2 v_{\mathbf{k}}(\mathbf{r}) V(\mathbf{k}) - |\psi_{\text{MF}}(\mathbf{r})|^2 u_{\mathbf{k}}(\mathbf{r}) V(\mathbf{k}) . \end{aligned} \quad (7)$$

In this expression, μ_{MF} is the mean field chemical potential, and $|\psi_{\text{MF}}(\mathbf{r})|^2$ is the mean-field density, i.e. the solution of Eq. 1 without accounting for beyond mean-field fluctuations. We can now use the exact identity for the mean field chemical potential

$$\mu_{\text{MF}} = -\frac{\hbar^2}{2m} \frac{\nabla^2 \psi_{\text{MF}}}{\psi_{\text{MF}}(\mathbf{r})} + U(\mathbf{r}) + \int d\mathbf{r}' V(\mathbf{r} - \mathbf{r}') |\psi_{\text{MF}}(\mathbf{r}')|^2 \quad (8)$$

to reach the equations

$$E_{\mathbf{k}} u_{\mathbf{k}}(\mathbf{r}) = \left(\frac{\hbar^2 k^2}{2m} + \frac{\hbar^2}{2m} \frac{\nabla^2 \psi_{\text{MF}}}{\psi_{\text{MF}}(\mathbf{r})} \right) u_{\mathbf{k}}(\mathbf{r}) + |\psi_{\text{MF}}(\mathbf{r})|^2 u_{\mathbf{k}}(\mathbf{r}) V(\mathbf{k}) - |\psi_{\text{MF}}(\mathbf{r})|^2 v_{\mathbf{k}}(\mathbf{r}) V(\mathbf{k}) \quad (9)$$

$$- E_{\mathbf{k}} v_{\mathbf{k}}(\mathbf{r}) = \left(\frac{\hbar^2 k^2}{2m} + \frac{\hbar^2}{2m} \frac{\nabla^2 \psi_{\text{MF}}}{\psi_{\text{MF}}(\mathbf{r})} \right) v_{\mathbf{k}}(\mathbf{r}) + |\psi_{\text{MF}}(\mathbf{r})|^2 v_{\mathbf{k}}(\mathbf{r}) V(\mathbf{k}) - |\psi_{\text{MF}}(\mathbf{r})|^2 u_{\mathbf{k}}(\mathbf{r}) V(\mathbf{k}) , \quad (10)$$

where $V(\mathbf{k})$ denotes the Fourier transform of the interaction, i.e.

$$V(\mathbf{k}) = \frac{4\pi\hbar^2 a}{m} + \frac{4\pi\hbar^2 a_{\text{dd}}}{m} \left(3 \frac{k_z^2}{k^2} - 1 \right) . \quad (11)$$

We now replace $|\psi_{\text{MF}}(\mathbf{r})|^2 \rightarrow \rho_0$ and build a density dependent function $F(\rho_0) = \frac{\hbar^2}{2m} \frac{\nabla^2 \psi_{\text{MF}}}{\psi_{\text{MF}}(\mathbf{r})}$ by expressing this quantity in terms of the mean-field density $|\psi_{\text{MF}}(\mathbf{r})|^2$. Since the thermal correction ignoring the condensate curvature has been proven successful in the reproduction of experimental results on dipolar systems at finite temperature [22], we assume a completely flat condensate near the center and only account for the curvature near the edges of the trap. This can be achieved by retaining the contribution of $F(\rho_0)$ for densities for which $F(\rho_0) > 0$ only. It turns out that in this regime $F(\rho_0)$ can be approximately fitted to the density functional form

$$F(\rho_0) = c_1 \ln(\rho_0) + c_2 \quad (12)$$

with c_1 and c_2 fitting parameters. This expression is exact for the ground state wave function of an isotropic harmonic oscillator. Thus, we solve the coupled equations

$$E_{\mathbf{k}} u_{\mathbf{k}} = \left(\frac{\hbar^2 k^2}{2m} + \tilde{F}(\rho_0) \right) u_{\mathbf{k}} + \rho_0 u_{\mathbf{k}} V(\mathbf{k}) - \rho_0 v_{\mathbf{k}} V(\mathbf{k}) \quad (13)$$

$$- E_{\mathbf{k}} v_{\mathbf{k}} = \left(\frac{\hbar^2 k^2}{2m} + \tilde{F}(\rho_0) \right) v_{\mathbf{k}} + \rho_0 v_{\mathbf{k}} V(\mathbf{k}) - \rho_0 u_{\mathbf{k}} V(\mathbf{k}) . \quad (14)$$

where $\tilde{F}(\rho_0) = \text{Max}\{F(\rho_0), 0\}$. Using $u_{\mathbf{k}}$ and $v_{\mathbf{k}}$ we can compute the thermal correction of Eq. 5, where the \mathbf{r} dependence stems from the substitution $\rho_0 \rightarrow |\psi(\mathbf{r})|^2$ in the excitation spectrum $\varepsilon_{\mathbf{k}}(\rho_0)$ and the Bogoliubov amplitudes.

C. Calculation of the density of thermal molecules

In order to solve Eq. 1 iteratively, we need to obtain the density of thermal molecules at each iteration. Within Bogoliubov theory, the thermal density of depleted molecules for an homogeneous system can be computed as (see Eq. 35 of Ref. [30])

$$\rho_{\text{th}} = \int \frac{d\mathbf{k}}{(2\pi)^3} \frac{1}{e^{\beta \epsilon_{\mathbf{k}}} - 1} \left(|u_{\mathbf{k}}|^2 + |v_{\mathbf{k}}|^2 \right) . \quad (15)$$

In order to obtain the depleted cloud of thermal molecules from Eq. 1, we compute ρ_{th} for different values of the condensate density of the homogeneous system, ρ_0 , thus building a density functional. Then, we solve Eq. 1 iteratively through imaginary time propagation and evaluate the thermal density at each point in space by computing $\rho_{\text{th}} \left(\rho_0 = |\psi(\mathbf{r})|^2 \right)$ i.e. we replace the homogeneous density by the value of the trapped density, as it is typically done in the LDA..

III. RESULTS

To match the conditions of the experiment of Ref. [6], the dipolar length is $a_{\text{dd}} = 1250a_0$ while the s -wave scattering length is set to $a = 1500a_0$, meaning that $\epsilon_{\text{dd}} = a_{\text{dd}}/a = 0.83 < 1$, so that dipolar effects are not dominant. The trap frequencies are $(\omega_x, \omega_y, \omega_z) = 2\pi(23, 49, 58)$ Hz. In what follows, we employ the characteristic length and energy scales set by $r_0 = 12\pi a_{\text{dd}}$ and $\epsilon = \hbar^2/(mr_0^2)$.

A. Condensate fraction

By numerically solving the TeGPE we can obtain the condensate wave function $\psi(\mathbf{r})$ as well as the depleted density $n_{\text{d}}(\mathbf{r})$. Since the gas lies in the dilute regime ($\rho a^3 < \rho_{\text{peak}} a^3 \simeq 7.2 \times 10^{-4}$ with ρ_{peak} the peak density), the quantum depletion of the condensate due to interaction effects is significantly smaller than the thermal one, within the range of experimental temperatures. With this theoretical approach, we can describe the formation of the dipolar molecular BEC as the temperature decreases, as shown in Fig. 1. The figure shows both the rise of a density peak and the tightening of the density distribution as more and more molecules fall into the condensate.

By fixing the total number of harmonically trapped molecules to the values of the experiment of Ref. [6], we can directly compare the TeGPE results for the condensate depletion with that measured in the experiment. We show the results in Fig. 2. Notice that each point in the figure corresponds to a different total number of particles as well as a different temperature, since the experimental measurements were taken during an evaporative cooling sequence. Remarkably, and as we can see from the figure, our result is in excellent agreement with the experimental prediction within the errorbars, even when the condensate fraction is as low as 20%. The agreement is expected to worsen at higher temperatures, as the theory is expected to be more accurate at low temperatures, when less excited states are populated. The good agreement between the eGPE and the experimental observations indicates that the system is in the universal regime, where the specific details of the molecular interaction do not significantly alter its properties. This means that,

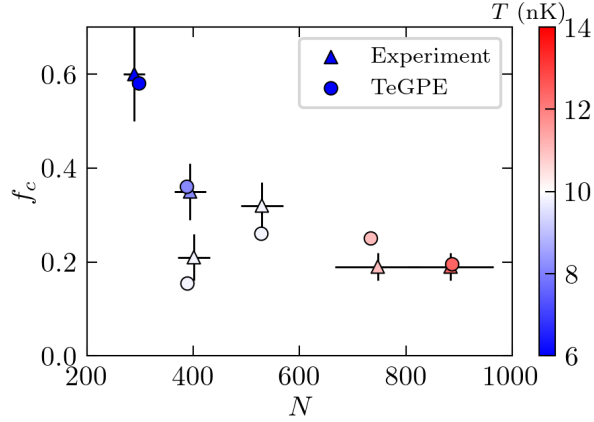


FIG. 2. Condensate fraction of the NaCs molecular condensate under the experimental conditions of Ref. [6]. The horizontal axis corresponds to the total number of molecules while the colorbar indicates the temperature.

in the weakly dipolar regime, the parameter that controls the physics of the system is the scattering length a . Furthermore, our results also stress the robustness of the finite temperature Bogoliubov theory for the description of dipolar systems in the contact-dominated regime, where $a > a_{dd}$. This accuracy is still present in the dipolar dominated regime ($a < a_{dd}$), where supersolids of ^{164}Dy atoms arise [22]. However, further decreasing the scattering length in a system of dipolar molecules, which in turn leads to higher densities, breaks the validity of the theory [7].

It must be stressed that, while our condensed fractions are computed from the lowest free energy solution of the trapped system, those of the experiment of Ref. [6] are obtained after a 17 ms TOF expansion. However, due to the comparatively large lifetime of the condensate, of the order of seconds (see Fig. 5 of Ref. [6]), the condensate fraction should remain unchanged after this expansion, which allows us to compute it and find excellent agreement without the need to perform a TOF expansion.

In Ref. [6], the condensate fraction is estimated by fitting a bimodal density distribution to the experimentally measured density profile after the expansion. The bimodal distribution is given by

$$\rho_{\text{fit}}(x) = \frac{15N_{\text{TF}}}{16\sigma_{\text{TF}}} \text{Max.} \left\{ 1 - \left(\frac{x - x_{\text{TF}}}{\sigma_{\text{TF}}} \right)^2, 0 \right\}^2 + \frac{N_{\text{G}}}{\sqrt{2\pi}\sigma_{\text{G}}} \exp \left(-\frac{(x - x_{\text{G}})^2}{2\sigma_{\text{G}}^2} \right), \quad (16)$$

where N_{TF} , N_{G} , σ_{TF} , σ_{G} , x_{TF} and x_{G} are fitting parameters. The first term on the r.h.s of Eq. 16 corresponds to the contribution of the condensate to the density while the second term accounts for the thermal density. Moreover, $\sigma_{\text{TF,G}}$ represents the width of the fit, $x_{\text{TF,G}}$ the centers, and $N_{\text{TF,G}}$ stand for the number of condensed and

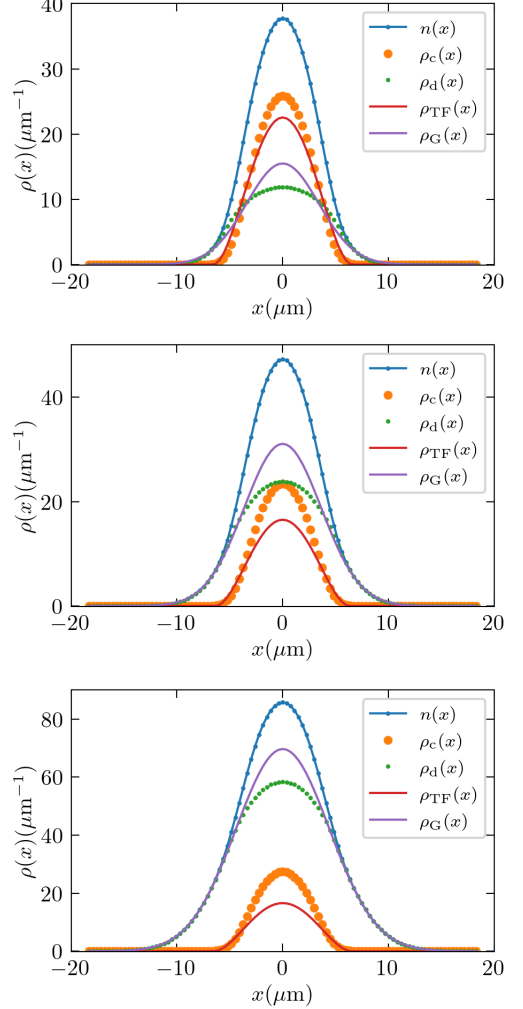


FIG. 3. Ground state column density $\rho(x)$, condensate density $\rho_c(x)$, and depleted density $\rho_d(x)$ of the molecular condensate at three different points of the experiment of Ref. [6]: ($N = 289, T = 6$ nK) (top), ($N = 394, T = 8.2$ nK) (middle), ($N = 884, T = 12.6$ nK) (bottom). We also include the gaussian and TF contributions of the bimodal fit of Eq. 16, which are obtained by fitting the total density.

thermally excited particles, respectively. The condensate fraction is then estimated as $f_c \simeq N_{\text{TF}}/(N_{\text{TF}} + N_{\text{G}})$. It is interesting to benchmark this procedure to obtain f_c by applying it to our theoretical density profiles and comparing the results with our TeGPE estimation for the same quantity. We show the results in Table I.

By solving the TeGPE, we can obtain the ground state density profiles, together with the condensate and excited density distributions. We can use our results to further benchmark the bimodal fit of Eq. 16 by comparing the shape of the condensate and thermal components to the fitting functions. We denote the gaussian and TF components of the fit of Eq. 16 as $\rho_{\text{TF}}(x)$ and $\rho_{\text{G}}(x)$, respectively, and show our results in Fig. 3. From both the figure and the data of Table I, we see that the bimodal

(N, T)	f_c^{TeGPE}	$f_{c,\text{fit}}^{\text{TeGPE}}$	$f_c^{\text{exp.}}$
(289, 6 nK)	0.58	0.54	0.6 ± 0.1
(394, 8.2 nK)	0.36	0.28	0.35 ± 0.06
(884, 12.4 nK)	0.195	0.156	0.19 ± 0.03

TABLE I. Condensate fraction obtained from the TeGPE calculations for different values of N and T corresponding to the experiment of Ref. [6]. f_c indicates the value computed by solving the TeGPE, $f_{c,\text{fit}}$ corresponds to the estimation applying the bimodal fit of Eq. 16 to the density profiles, and $f_c^{\text{exp.}}$ denotes the experimental values.

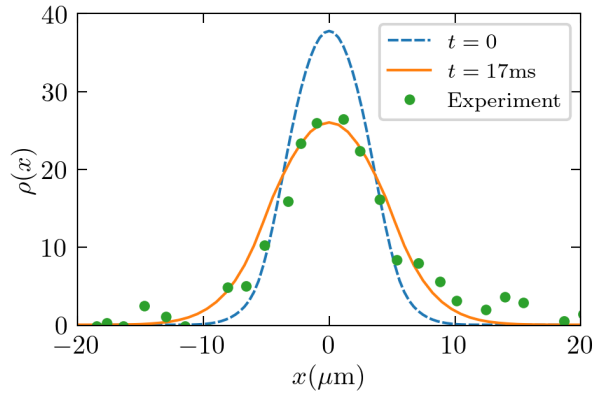


FIG. 4. Ground state (dashed line) and time-evolved density profiles (solid line) obtained, respectively, from the solution of the TeGPE and the tTeGPE. The time evolution corresponds to a 17 ms TOF expansion. Dots indicate the experimental density distribution of Ref. [6]. The number of particles is $N = 289$ while the temperature is $T = 6$ nK.

fit consistently and slightly underestimates the condensate fraction, although it lays indeed close to the computed condensate fractions when applied to the TeGPE profiles.. Regardless, we see that the fit quantitatively captures the width of the condensate and depleted distributions, and also gives a solid approximation of the density at the center of each distribution.

Our formalism is capable of estimating the critical temperature of the condensate for a fixed total number of molecules N . This is done by solving Eq. 1 at different temperatures to find the one for which $N = N_d$, with N_d the number of depleted molecules. To further characterize the coldest condensate obtained in the experiment of Ref. [6], we perform calculations for a system of $N = 289$ particles and find that the condensate should disappear at $T \simeq 9.8$ nK.

B. Density profiles after TOF

To further characterize the system, one can have a look at the molecular density profile. As stated previously, in the experiment of Ref. [6], the column densities of the molecular cloud are measured after a TOF expansion of 17 ms. To compare our density profiles with the experi-

mental ones, therefore, we need to simulate this TOF expansion. Solving the TeGPE in the presence of the trap allows us to find the lowest free-energy quantum state. Subsequently, taking its solution as an initial state, we can approximately simulate the TOF expansion of the system by solving the time-dependent TeGPE (tTeGPE) when the trap is removed, which is given by

$$i\hbar \frac{\partial \psi}{\partial t} = \left(-\frac{\hbar^2 \nabla^2}{2m} + U(\mathbf{r}) \right. \\ \left. + \int d\mathbf{r}' V(\mathbf{r} - \mathbf{r}') \left(|\psi(\mathbf{r}', t)|^2 + \rho_d(\mathbf{r}', t) \right) \right. \\ \left. + H_{\text{qu}}(\mathbf{r}, t) + H_{\text{th}}(\mathbf{r}, t) \right) \psi(\mathbf{r}, t) \quad (17)$$

$$= \hat{K}\psi(\mathbf{r}, t) + \hat{V}_{\text{TeGPE}}(\mathbf{r}, t)\psi(\mathbf{r}, t). \quad (18)$$

where $\hat{K} = \frac{\hat{P}^2}{2m}$ is the kinetic energy operator. In principle, this equation must be solved simultaneously while numerically performing the time evolution of the non-condensed density $\rho_d(\mathbf{r}, t)$, which is governed by the time-dependent Bogoliubov equations. However, the depleted cloud is obtained under the local density approximation, which ignores the trapping potential away from the low-density regions. Since the Hamiltonian that is used in the time-evolution has the trapping potential removed, we assume that the depleted cloud remains unchanged during the TOF expansion, and compute the time evolution of the condensate component by solving Eq. 17 for the static distribution of non-condensed molecules.

In practice, to implement the real-time evolution, we apply the time-evolution operator to the wave function iteratively, which we split as

$$\hat{O}_t \simeq \exp \left[-i \frac{\hat{V}_{\text{TeGPE}} \Delta t}{2\hbar} \right] \exp \left[-i \frac{\hat{K} \Delta t}{\hbar} \right] \exp \left[-i \frac{\hat{V}_{\text{TeGPE}} \Delta t}{2\hbar} \right], \quad (19)$$

which is exact up to order Δt^2 . If the time step is small enough, we can use the initial state at every iteration to compute $V_{\text{TeGPE}}(\mathbf{r}, t)$, which depends on the density. The terms of the propagator which contain the potential are applied in position space, while the kinetic term is applied in momentum space by using an FFT algorithm.

We show in Fig. 4 the tTeGPE result after the TOF expansion, together with the TeGPE ground state and post-TOF experimental density distributions, for the coldest point recorded in the experiment ($N = 289$, $T = 6$

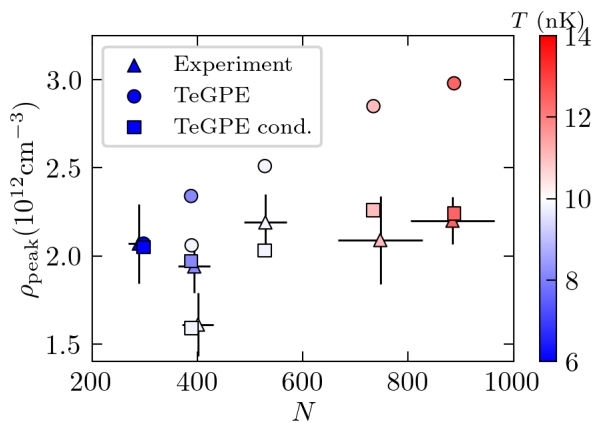


FIG. 5. Peak density of the molecular condensate under the experimental conditions of Ref. [6]. The horizontal axis corresponds to the total number of particles while the colorbar indicates the temperature. The “TeGPE” results correspond to the peak density of the total cloud obtained from a TeGPE simulation, while the “TeGPE cond.” results correspond to the peak density of the condensate molecules alone. Note that the experimental estimation does not account for the effect of the DDI nor the thermal cloud [6, 34].

nK). Remarkably, we obtain an excellent agreement between theory and experiment. Moreover, we see that, for the case shown, where the condensate fraction is $f_c \simeq 0.6$, the expansion dynamics are mostly governed by the molecules in the condensate, despite the presence of a significant thermal cloud.

C. Peak density

We estimate the peak density from the ground state density profiles (no TOF expansion is performed) and compare it to the experimental results in Fig. 5. It must be remarked that the authors in Ref. [6] use the number of condensed molecules after the TOF expansion to obtain the peak density of the system before the expansion. They use the expression

$$\rho_{\text{peak}} = \frac{15^{2/5}}{8\pi} \left[m^3 \bar{\omega}^3 N_c / \left(\hbar^3 a^{3/2} \right) \right]^{2/5}. \quad (20)$$

where N_c is the number of condensed molecules and $\bar{\omega} = \sqrt{\omega_x \omega_y \omega_z}$ is the geometric mean of the trapping frequencies. This expression ignores both the effect of the DDI, as well as the presence of the thermal cloud [34]. From the results, we see that the TeGPE estimates lay relatively close to the experimental ones for the highest values of the condensate fraction, while the agreement worsens for the largest temperatures/lowest condensate fractions, mainly due to the experimental results neglecting the thermal cloud. Because of this, we also include the values for the peak density of the condensate alone

(squares in Fig. 5). In this case, we find excellent agreement with the experimental results at all temperatures.

D. The pseudopotential and the inter-molecular interaction under double MW shielding

The full nature of the inter-molecular interaction in the experiment is not disclosed in Ref. [6]. However, Refs. [35, 36] shed more light into this question. The long range part of the interaction between molecules under a circularly polarized MW field σ^+ and a linearly polarized MW field π can be expanded in spherical harmonics (see Eq. 24 of Ref. [35])

$$V_{\text{long}}(\mathbf{r}) = -2 \sum_m (d_{\text{eff}}^m)^2 \frac{Y_2^m(\theta, \phi)}{4\pi\epsilon_0 r^3} \quad (21)$$

where \mathbf{r} is the relative position vector between two molecules, θ and ϕ are the polar and azimuthal angles and $Y_2^m(\theta, \phi)$ is the $l = 2, m$ spherical harmonic. The z -axis is taken here as the direction of the polarization. Using the convention of Ref. [35], the effective dipole moment in Eq. 21 can be either a real or an imaginary number, depending on the sign of the effective dipole length $a_{dd}^m = m(d_{\text{eff}}^m)^2 / (12\pi\hbar^2\epsilon_0)$ associated to each partial wave channel. In the absence of ellipticity, the interaction is just given by the $m = 0$ term, while the magnitude and sign of the effective dipole length a_{dd}^0 can be changed by tuning the Rabi frequencies and detunings of the MW fields (it can also be completely cancelled) [35, 36]. Thus, in this case, the long range part of the interaction corresponds to the standard dipole-dipole interaction (DDI) for dipoles polarized along the z -axis for $a_{dd}^0 > 0$ and the anti-dipolar interaction for $a_{dd}^0 < 0$. In this sense, the interaction employed in our work matches the inter-molecular interaction for zero ellipticity and $a_{dd}^0 > 0$. In this case, we can relate the effective dipole moment $d_{\text{eff}}^{(0)}$ with the Rabi frequencies and detunings employed in the experiments to achieve the double MW shielding. By comparing Eq. 21 with Eq. (21) of Ref. [36] we obtain

$$d_{\text{eff}}^{(0)} = \sqrt{-\frac{1}{3} \sqrt{\frac{\pi}{5}} d^2 (3 \cos(2\beta) - 1) \cos^2 \alpha \sin^2 \alpha}. \quad (22)$$

where d is the bare dipole moment of the molecules and α and β are two Euler angles, which depend on the detunings $(\delta_\sigma, \delta_\pi)$ and Rabi frequencies $(\Omega_\sigma, \Omega_\pi)$ of the σ^+ and π polarized fields. These Euler angles arise from the diagonalization of the single molecule Hamiltonian under the presence of the aforementioned fields and their dependence on the parameters $\Omega_\sigma, \Omega_\pi, \delta_\sigma, \delta_\pi$ is not analytical.

While we have assumed the dipoles to be polarized along the z -axis, the polarization direction of the dipoles in the experiment is unknown, as mentioned in the supplementary information of Ref. [6]. In order to quantify the effect of the polarization in our results, we have

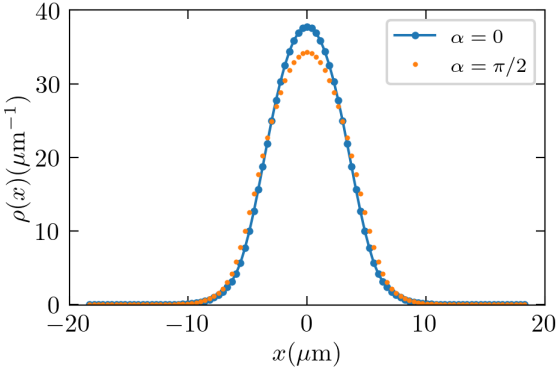


FIG. 6. Ground state density distribution of the molecular condensate for the coldest experimental point ($N = 289$, $T = 6$ nK, $\epsilon_{\text{dd}} = 0.83$) for a system of dipoles polarized along the z -axis ($\alpha = 0$, blue line with markers), and for a system polarized along the x -axis ($\alpha = \pi/2$, orange markers). Here α is the tilting angle of the dipoles in the x - z plane

performed calculations at the coldest experimental point ($N = 289$, $T = 6$ nK) for a system of dipoles polarized along the x -axis (see Fig. 6). Our results show that the TeGPE density profile is only slightly affected by drastically changing the polarization. Moreover, the condensate depletion is only modified by $\simeq 0.01$. This means that the uncertainty in the polarization direction does not change the physical picture presented in this work.

Lastly, the short range part of the full inter-molecular potential corresponds to a term decaying with the inter-molecular distance as $\sim 1/r^6$ and anisotropic, with a dependence on θ at zero ellipticity [36]. In our work, we have considered a pseudopotential of the form [7, 37]

$$V(\mathbf{r}) = \frac{4\pi\hbar^2 a}{m} \delta(\mathbf{r}) + V_{\text{dd}}(\mathbf{r}) \quad (23)$$

with $V_{\text{dd}}(\mathbf{r})$ given in Eq. 2. This is a good approximation as long as the generalized scattering lengths, $a_l^{m=0}$ are insensitive to the anisotropy of the short range potential for $l > 0$ (see Ref. [38]). While we can not explicitly check this, because we do not have access to the full inter-molecular potential, we performed T-matrix calculations employing the inter-molecular potential under a single, circularly polarized MW field of Ref. [38] and checked that these scattering lengths are unaffected by the short range anisotropy. Therefore, it is reasonable to assume the same will happen for the doubly MW shielded interaction at zero ellipticity, since the dependence on the inter-molecular distance of the short and long range parts of the interaction is the same, and there is only anisotropy through a dependence on θ in both cases. Thus, we can argue that the pseudopotential employed in our work is accurate enough to describe the experimental system.

IV. CONCLUSIONS

In conclusion, we have employed the temperature-dependent extended Gross-Pitaevskii equation to theoretically model the condensate of dipolar molecules of Ref. [6]. We have reported calculations for the condensate fraction that are in excellent agreement with the experimental values. We have also obtained excellent agreement with the experimental density profile after a 17 ms TOF expansion in the coldest experimental conditions, where the condensate fraction is the highest. Moreover, we have reported results for the peak density of the condensate component, and find excellent agreement between our results and the experimental ones, which neglect the presence of the thermal cloud. We also provide the values of the peak density accounting for the presence of such thermal density of depleted molecules.

Our results, thus, establish the validity of Bogoliubov theory and the TeGPE for the description of the very novel molecular condensates in the dilute regime, away from strong dipolar interactions, which need exact *ab initio* methods like quantum Monte Carlo algorithms to properly be described [7]. Even in the regime considered in this work, slight quantitative improvements in regards to the density profiles and peak densities could be achieved by means of quantum Monte Carlo simulations, which are able to exactly account for the excited thermal cloud. Moreover, the use of these methods can also allow for the quantification of the superfluid density present in the system.

We believe that the control of dipolar molecular condensates will open interesting research avenues in the near future. Future work should address the study of dipolar molecules in the strongly dipolar regime, where the enhanced dipolar moment will play a dominant role. Although it is difficult to anticipate all the possibilities that these systems will offer, a direct comparison with magnetic atom setups can give us some insight. Firstly, as it happens with dipolar atoms, the formation of self-bound molecular clusters (droplets) is expected to occur. However, the critical number of molecules to form them can be up to ten times smaller than the one observed in experiments with Dy and Er atoms [7]. And secondly, while a supersolid state formed by arrays of atomic clusters has been experimentally realized, it is still unclear if the smaller, and more correlated, molecular dipolar clusters are able to maintain phase coherence between them or, on the contrary, they will form an insulating state. Finally, in dipolar condensates of magnetic atoms, it has been observed that a supersolid state can be reached after heating a gaseous BEC by increasing the temperature in the nK regime [21]. Thus, a third important line of research will be to elucidate whether the balance between thermal fluctuations, quantum correlation and anisotropic interaction can lead to the observation of similar exotic phenomena in molecular dipolar condensate.

We acknowledge financial support

from Ministerio de Ciencia e Innovación MCIN/AEI/10.13039/501100011033 (Spain) under Grant No. PID2023-147469NB-C21 and from AGAUR-Generalitat de Catalunya Grant No. 2021-SGR-01411. R.B. acknowledges funding from ADAGIO (Advanced

Manufacturing Research Fellowship Programme in the Basque – New Aquitaine Region) MSCA COFUND Post-Doctoral fellowship programme (Grant agreement No. 101034379).

[1] A. V. Gorshkov, P. Rabl, G. Pupillo, A. Micheli, P. Zoller, M. D. Lukin, and H. P. Büchler, “Suppression of inelastic collisions between polar molecules with a repulsive shield,” *Phys. Rev. Lett.* **101**, 073201 (2008).

[2] Junyu Lin, Guanghua Chen, Mucan Jin, Zhaopeng Shi, Fulin Deng, Wenxian Zhang, Goulven Quéméner, Tao Shi, Su Yi, and Dajun Wang, “Microwave shielding of bosonic narb molecules,” *Phys. Rev. X* **13**, 031032 (2023).

[3] Charbel Karam, Romain Vexiau, Nadia Bouloufa-Maafa, Olivier Dulieu, Maxence Lepers, Mara Meyer zum Alten Borgloh, Silke Ospelkaus, and Leon Karpa, “Two-photon optical shielding of collisions between ultracold polar molecules,” *Phys. Rev. Res.* **5**, 033074 (2023).

[4] Niccolò Bigagli, Claire Warner, Weijun Yuan, Siwei Zhang, Ian Stevenson, Tijs Karman, and Sebastian Will, “Collisionally stable gas of bosonic dipolar ground-state molecules,” *Nature Physics* **19**, 1579–1584 (2023).

[5] Bijit Mukherjee and Jeremy M. Hutson, “Controlling collisional loss and scattering lengths of ultracold dipolar molecules with static electric fields,” *Phys. Rev. Res.* **6**, 013145 (2024).

[6] Niccolò Bigagli, Weijun Yuan, Siwei Zhang, Boris Bulatovic, Tijs Karman, Ian Stevenson, and Sebastian Will, “Observation of bose–einstein condensation of dipolar molecules,” *Nature* **631**, 289–293 (2024).

[7] Tim Langen, Jordi Boronat, Juan Sánchez-Baena, Raúl Bombín, Tijs Karman, and Ferran Mazzanti, “Dipolar droplets of strongly interacting molecules,” *Phys. Rev. Lett.* **134**, 053001 (2025).

[8] Holger Kadau, Matthias Schmitt, Matthias Wenzel, Clarissa Wink, Thomas Maier, Igor Ferrier-Barbut, and Tilman Pfau, “Observing the rosenzweig instability of a quantum ferrofluid,” *Nature* **530**, 194–197 (2016).

[9] Matthias Schmitt, Matthias Wenzel, Fabian Böttcher, Igor Ferrier-Barbut, and Tilman Pfau, “Self-bound droplets of a dilute magnetic quantum liquid,” *Nature* **539**, 259–262 (2016).

[10] Igor Ferrier-Barbut, Holger Kadau, Matthias Schmitt, Matthias Wenzel, and Tilman Pfau, “Observation of quantum droplets in a strongly dipolar bose gas,” *Phys. Rev. Lett.* **116**, 215301 (2016).

[11] L. Chomaz, S. Baier, D. Petter, M. J. Mark, F. Wächtler, L. Santos, and F. Ferlaino, “Quantum-fluctuation-driven crossover from a dilute bose-einstein condensate to a macrodroplet in a dipolar quantum fluid,” *Phys. Rev. X* **6**, 041039 (2016).

[12] Fabian Böttcher, Matthias Wenzel, Jan-Niklas Schmidt, Mingyang Guo, Tim Langen, Igor Ferrier-Barbut, Tilman Pfau, Raúl Bombín, Joan Sánchez-Baena, Jordi Boronat, and Ferran Mazzanti, “Dilute dipolar quantum droplets beyond the extended gross-pitaevskii equation,” *Phys. Rev. Res.* **1**, 033088 (2019).

[13] L. Tanzi, E. Lucioni, F. Famà, J. Catani, A. Fioretti, C. Gabbanini, R. N. Bisset, L. Santos, and G. Modugno, “Observation of a dipolar quantum gas with metastable supersolid properties,” *Phys. Rev. Lett.* **122**, 130405 (2019).

[14] Fabian Böttcher, Jan-Niklas Schmidt, Matthias Wenzel, Jens Hertkorn, Mingyang Guo, Tim Langen, and Tilman Pfau, “Transient supersolid properties in an array of dipolar quantum droplets,” *Phys. Rev. X* **9**, 011051 (2019).

[15] L. Chomaz, D. Petter, P. Ilzhöfer, G. Natale, A. Trautmann, C. Politi, G. Durastante, R. M. W. van Bijnen, A. Patscheider, M. Sohmen, M. J. Mark, and F. Ferlaino, “Long-lived and transient supersolid behaviors in dipolar quantum gases,” *Phys. Rev. X* **9**, 021012 (2019).

[16] L. Tanzi, S. M. Rocuzzo, E. Lucioni, F. Famà, A. Fioretti, C. Gabbanini, G. Modugno, A. Recati, and S. Stringari, “Supersolid symmetry breaking from compressional oscillations in a dipolar quantum gas,” *Nature* **574**, 382–385 (2019).

[17] Mingyang Guo, Fabian Böttcher, Jens Hertkorn, Jan-Niklas Schmidt, Matthias Wenzel, Hans Peter Büchler, Tim Langen, and Tilman Pfau, “The low-energy goldstone mode in a trapped dipolar supersolid,” *Nature* **574**, 386–389 (2019).

[18] L. Tanzi, J. G. Maloberti, G. Biagioni, A. Fioretti, C. Gabbanini, and G. Modugno, “Evidence of superfluidity in a dipolar supersolid from nonclassical rotational inertia,” *Science* **371**, 1162–1165 (2021).

[19] Matthew A. Norcia, Claudia Politi, Lauritz Klaus, Elena Poli, Maximilian Sohmen, Manfred J. Mark, Russell N. Bisset, Luis Santos, and Francesca Ferlaino, “Two-dimensional supersolidity in a dipolar quantum gas,” *Nature* **596**, 357–361 (2021).

[20] Giulio Biagioni, Nicolò Antolini, Aitor Alaña, Michele Modugno, Andrea Fioretti, Carlo Gabbanini, Luca Tanzi, and Giovanni Modugno, “Dimensional crossover in the superfluid-supersolid quantum phase transition,” *Phys. Rev. X* **12**, 021019 (2022).

[21] Maximilian Sohmen, Claudia Politi, Lauritz Klaus, Lauriane Chomaz, Manfred J. Mark, Matthew A. Norcia, and Francesca Ferlaino, “Birth, life, and death of a dipolar supersolid,” *Phys. Rev. Lett.* **126**, 233401 (2021).

[22] J. Sánchez-Baena, C. Politi, F. Maucher, F. Ferlaino, and T. Pohl, “Heating a dipolar quantum fluid into a solid,” *Nature Communications* **14**, 1868 (2023).

[23] J. Sánchez-Baena, T. Pohl, and F. Maucher, “Superfluid-supersolid phase transition of elongated dipolar bose-einstein condensates at finite temperatures,” *Phys. Rev. Res.* **6**, 023183 (2024).

[24] Liang-Jun He, Juan Sánchez-Baena, Fabian Maucher, and Yong-Chang Zhang, “Accessing elusive two-dimensional phases of dipolar bose-einstein condensates by finite temperature,” *Phys. Rev. Res.* **7**, 023019 (2025).

[25] Mingwu Lu, Nathaniel Q. Burdick, Seo Ho Youn, and

Benjamin L. Lev, “Strongly dipolar bose-einstein condensate of dysprosium,” *Phys. Rev. Lett.* **107**, 190401 (2011).

[26] K. Aikawa, A. Frisch, M. Mark, S. Baier, A. Rietzler, R. Grimm, and F. Ferlaino, “Bose-einstein condensation of erbium,” *Phys. Rev. Lett.* **108**, 210401 (2012).

[27] S. Giorgini, L. P. Pitaevskii, and S. Stringari, “Thermodynamics of a trapped bose-condensed gas,” *Journal of Low Temperature Physics* **109**, 309–355 (1997).

[28] Abdelâali Boudjemâa, “Quantum dilute droplets of dipolar bosons at finite temperature,” *Annals of Physics* **381**, 68–79 (2017).

[29] Abdelâali Boudjemâa, “Fluctuations and quantum self-bound droplets in a dipolar bose-bose mixture,” *Phys. Rev. A* **98**, 033612 (2018).

[30] E. Aybar and M. Ö. Oktel, “Temperature-dependent density profiles of dipolar droplets,” *Phys. Rev. A* **99**, 013620 (2019).

[31] S. F. Öztürk, Enes Aybar, and M. Ö. Oktel, “Temperature dependence of the density and excitations of dipolar droplets,” *Phys. Rev. A* **102**, 033329 (2020).

[32] Aristeu R P Lima and Axel Pelster, “Quantum fluctuations in dipolar Bose gases,” *Physical Review A* **84**, 041604–4 (2011).

[33] A. R. P. Lima and A. Pelster, “Beyond mean-field low-lying excitations of dipolar bose gases,” *Phys. Rev. A* **86**, 063609 (2012).

[34] Franco Dalfovo, Stefano Giorgini, Lev P. Pitaevskii, and Sandro Stringari, “Theory of bose-einstein condensation in trapped gases,” *Rev. Mod. Phys.* **71**, 463–512 (1999).

[35] Tijs Karman, Niccolò Bigagli, Weijun Yuan, Siwei Zhang, Ian Stevenson, and Sebastian Will, “Double microwave shielding,” (2025), arXiv:2501.08095 [cond-mat.quant-gas].

[36] Fulin Deng, Xinyuan Hu, Wei-Jian Jin, Su Yi, and Tao Shi, “Two- and many-body physics of ultracold molecules dressed by dual microwave fields,” (2025), arXiv:2501.05210 [cond-mat.quant-gas].

[37] Abdelâali Boudjemâa, “Nonequilibrium quench dynamics of bose-einstein condensates of microwave-shielded polar molecules,” *Phys. Rev. A* **111**, 063315 (2025).

[38] S. Yi and L. You, “Trapped condensates of atoms with dipole interactions,” *Phys. Rev. A* **63**, 053607 (2001).